Relationship between macroscopic physical properties and local distortions of low-doping La$_{1-x}$Ca$_x$MnO$_3$: An EXAFS study

Y. Jiang,[1] F. Bridges,[1] L. Downward,[1] and J. J. Neumeier[2]

[1]*Physics Department, University of California, Santa Cruz, California 95064, USA*
[2]*Department of Physics, Montana State University, Bozeman, Montana 59717, USA*

A temperature-dependent extended x-ray-absorption fine structure investigation of La$_{1-x}$Ca$_x$MnO$_3$ is presented for the concentration range that spans the ferromagnetic-insulator (FMI) to ferromagnetic-metal (FMM) transition region, x=0.16, 0.18, 0.20, and 0.22; the titrated hole concentrations are slightly higher, y=0.2, 0.22, 0.24, and 0.25, respectively. For this range of Ca concentrations the samples are insulating for x=0.16–0.2 and show a metal/insulator (M/I) transition for x=0.22. All samples are ferromagnetic although the saturation magnetization for the 16% Ca sample is only $\sim$70% of the expected value at 0.4 T. This raises a question as to the nature of the ferromagnetic coupling mechanism in such insulating samples. We find that the FMI samples have similar correlations between changes in the local Mn-O distortions and the magnetization as observed previously for the colossal magnetoresistance (CMR) samples ($0.2 \leq x \leq 0.5$)—except that the FMI samples never become fully magnetized. The data show that there are at least two distinct types of distortions. The initial distortions removed as the insulating sample becomes magnetized are small and provide direct evidence that roughly 50% of the Mn sites (associated with the hole charge carriers) have a small average distortion/site and are magnetized first. The large Mn-O distortions that remain at low T are attributed to a small fraction ($<$30%) of fully Jahn-Teller-distorted Mn sites that are either unmagnetized or antiferromagnetically ordered. Thus the insulating samples are very similar to the behavior of the CMR samples up to the point at which the M/I transition occurs for the CMR materials. The lack of metallic conductivity for $x \leq 0.2$, when 50% or more of the sample is magnetic, implies that there must be preferred magnetized Mn sites (that involve holes) and that such sites do not percolate at these concentrations.

I. INTRODUCTION

LaMnO$_3$ is an antiferromagnetic insulator and has a large Jahn-Teller (JT) distortion of the MnO$_6$ octahedron. When it is doped with Ca on the La sites [i.e., La$_{1-x}$Ca$_x$MnO$_3$ (LCMO)], holes are introduced into the Mn e_g band and this leads to novel transport and magnetic properties including colossal magnetoresistance (CMR) and ferromagnetism for samples with Ca concentrations x roughly in the range 20–50 %.[1–3] In this concentration range, these pseudocubic manganites are paramagnetic insulators (semiconductors) at high T, with a significant distortion of the Mn-O octahedron (for some sites) that is associated with Jahn-Teller distortions and polarons. Upon lowering the temperature below the ferromagnetic transition temperature T_c, the Mn spins begin to align and thus the holes (electrons) can hop more rapidly between Mn atoms without a spin flip via the intervening O atom; this enhances the ferromagnetic (FM) coupling between Mn spins and is referred to as the double exchange (DE) interaction.[4–6] To explain the large magnetoresistance a Jahn-Teller-type polaron lattice distortion must also be present.[7–11] A consequence of very fast hopping of holes between neighboring Mn sites is that the broadening σ of the Mn-O pair distribution function (PDF) is greatly reduced when the sample becomes magnetic, thus $\sigma^2(T)$ decreases rapidly below the ferromagnetic transition temperature T_c. Finally, at low T, LCMO in the CMR regime is a ferromagnetic metal with very little static distortion of the Mn-O bonds.[12–14]

For LCMO in this concentration range ($x \sim 0.2–0.5$), Downward *et al.*[14] have shown that there is a strong correlation between the local Mn-O distortions removed, $D = \Delta(\sigma^2)$, and the magnetization, as T is lowered through and below T_c. By plotting D (for the Mn-O PDF) versus the sample magnetization, Downward *et al.*[14] found that D increases slowly with M until $M/M_0 \sim 2x$ (M_0 is the saturation magnetization at low T); for larger M, D increases more rapidly. The low initial slope in such a plot is experimental evidence for sites with a low average distortion/site, while the large slope [$\sim$3–4 times larger for x=0.3 (Ref. 14)] at high M indicates that the remaining smaller fraction of Mn sites has a large distortion/site. Thus there are at least two different types of average distortion present, which have only been distinguished (so far) by correlating with magnetization. An important question is—can one of the regimes be made more dominant by appropriate doping, so that this effect is more directly observable? We will address that issue in this paper.

Because the fraction of low-distortion sites is roughly $2x$, Downward *et al.*[14] proposed a two-site polaron model (called a dimeron) in which a hole is partially delocalized over two Mn sites [initially one Mn site would correspond to an e_g electron site (Mn^{+3}) while the other would correspond to a hole site (Mn^{+4})]. The argument for a lower distortion within this two-site dimeron model is that when the hole (or electron) is partially delocalized—a dynamic effect—the average charge per site is reduced to 3.5 (from four electrons on an isolated Mn^{+3} site), JT energies are reduced, and the corresponding JT distortion is smaller. However, Downward *et al.* also pointed out that one could explain the results with a varying distortion around the polaron.

In either case, the magnetization M first develops via the aggregation of the lowest average-distortion sites, while for large M, further increases in M (induced by either lowering T or increasing B) force the remaining high-distortion sites (likely fully JT-distorted Mn sites), to become magnetized and the hole quasiparticles now visit these sites. For the CMR samples, *most* of the distortion removed in the FM state occurs *after* the sample is more than 50% magnetized.[14]

Consequently, if the sample never became fully magnetized, e.g., for the lower Ca concentrations considered here, the remaining net Mn-O distortion at low T should be much larger than has been observed for the CMR regime. Note that in the partially magnetized state at low M there will be three types of Mn sites—(i) undistorted sites in the developing magnetic regions, (ii) some of the low average-distortion sites (the remaining dimerons within that model) that are not yet part of a magnetic cluster, and (iii) highly distorted Mn^{+3} sites.

In considering how double exchange leads to both ferromagnetism and a disappearance of local Mn-O distortions, an important question to ask is how many Mn sites can one hole keep undistorted by hopping rapidly between them in the ferromagnetic metallic phase? The answer appears to be about four. For the 25% Ca samples, there are four sites/hole, (for higher Ca concentrations fewer sites/hole). The material is ferromagnetic and there is little excess distortion at low T for x between 25 and 40% (Refs. 13 and 14)—the Mn-O distortion at low T approaches the zero-point-motion value comparable to that observed in $CaMnO_3$. For lower Ca concentrations, there is an increasing amount of distortion at low T and at $x=0.21$ the sample does not become fully magnetic even at moderate fields (0.4 T).[14] Thus in this case the holes do not get to every site often enough to maintain all the sites at a low distortion.

A related point is that dynamics plays an important role; if the holes hop fairly rapidly above T_c—at least among a few sites—then there will be no Mn^{+4} sites in the sample over the time scale of most experiments. Thus characteristics of a particular site become a time average of a hole site and an electron site as holes hop on and off that particular site. This will depend on the time scale of the measurements and the hole hopping rate; the latter exceeds optical phonon frequencies in the ferromagnetic-metal (FMM) regime. When the hole is present the site becomes less distorted, whereas when an e_g electron is present it will become more distorted; consequently, rapid hopping at the local level will produce a lower net distortion per site, at least for some sites.

At lower Ca concentrations it is well known that the material becomes a ferromagnetic insulator (semiconductor) at low T.[1] An important detail is that these samples are never fully magnetized in moderate fields at low T, and the unmagnetized fraction increases slowly as the Ca concentration decreases below $\sim 20\%$ Ca. Since LCMO is a soft ferromagnet for higher Ca concentrations it is fully magnetized at low T for moderate fields (0.4 T)[14,15] and as we will show, for all the samples studied here that have a M/I transition. At lower Ca concentrations ($x \sim 0.1$) a canted antiferromagnetic (AFM) state exists[16,17] but disappears near $x=0.125$.[16] However, that does not preclude tiny AFM coupled clusters a few nm in size whose size diminishes as x approaches 0.22. Thus

the nature of the magnetic structure is not well understood in this concentration range.

At first ferromagnetism in an insulator appears to be in contradiction to a DE model,[18–20] because for double exchange, the Mn spins are ferromagnetically coupled via fast hopping of the holes (or e_g electrons) between Mn sites in the metallic regime. Some have suggested a mixture of (DE) ferromagnetic metallic and ferromagnetic insulating (distorted and nonconducting) phases,[19,21,22] but that requires invoking a new FM coupling mechanism (FM superexchange) for the FMI phase (for only a tiny change in Ca concentration), although the superexchange mechanism is normally AFM in $LaMnO_3$. That may well be necessary at low concentrations ($x=0.1$) where there are not enough holes to couple all the Mn sites via DE (the ratio is now 10 Mn sites/hole). Interestingly, the $x=0.1$ sample can be made completely ferromagnetic but nonconducting in a 12 T field;[22] however, in that case there should be a significant fraction of the sample that is magnetized and yet retains a large JT distortion since the latter is only removed if the hole quasiparticles are hopping rapidly over all the sites. One alternative explanation for a low magnetization at moderate fields for concentrations near 16–20 % is that FM (conducting) domains do form but are separated by insulating, nonferromagnetic regions (possibly tiny antiferromagnetically coupled clusters or a frustrated spin-glass-like configuration as a result of competing FM and AFM magnetic interactions for some sites). In either case, for x near 20% a small fraction of the sample appears to block the metallic conductivity and appears to be due to the intrinsic inhomogeneity of the sample at the unit cell level.

Several other papers also speak to this inhomogeneity. Electron magnetic resonance (EMR) studies[23,24] indicate multiple phases in a sample close to the concentration-driven M/I transition. For $x=0.18$ and 0.2 they observe at least three resonance lines,[24] which they attribute to different phases just below T_c—a ferromagnetic metallic phase and two distinct ferromagnetic insulating phases. Other investigations at low Ca concentrations suggest that Mn^{+4} hole sites may be localized. Alonso *et al.*[15] argue that in such samples, the conductive properties depend on the origin of the holes— from metal atom vacancies or from Ca dopants; the samples need Ca dopants to be conducting at higher concentrations. They propose that localized Mn^{+4} hole sites form close to the Ca dopants, which leads to unconnected magnetic/metallic clusters at low Ca concentrations; they also suggest that perhaps the JT distortions of Mn^{+3} sites near the Ca^{+2} dopants are smaller than near La^{+3}, but they do not provide a well defined model. Algarabel *et al.*[22] also suggest that holes are likely found close to the Ca sites in low concentration samples. Finally, in zero-field NMR experiments using low Ca concentration samples, at least three distinct regions with different hyperfine fields at the Mn nuclei have been observed, but only at very low T when the magnetization has reached it's maximum value;[21] they do not report results in the temperature regime (100–200 K) over which most of the magnetization develops. They argue that a significant fraction of (localized) Mn^{+4} are FM coupled. This requires a different FM coupling mechanism to produce insulating FM Mn^{+4} sites and essentially no hopping of such holes.

Finally, it should be noted that diffraction studies[16,17] suggest a transition for low Ca concentrations from a high temperature pseudocubic to a low temperature, lower symmetry phase, with the transition between 200 and 400 K. Biotteau *et al.*[16] interpreted this transition as an evolution from a dynamic Jahn-Teller effect (high T) to a cooperative static JT distortion (space group *Pbnm*) at lower T. A more recent paper[17] describes this transition as a symmetry change at T_{JT} from $P2_1/c$ at low T to orthorhombic (*Pnma*) at high T. For example, for the $x=0.175$ sample, Pissas *et al.*[17] show that the separation of the Mn-O bond lengths is a maximum near 200 K for $P2_1/c$; the distribution of bond lengths narrows slightly at low T but collapses to essentially one bond length at 300 K. This is in contrast to the EXAFS results we present here for which the distortions remain large at 300 K. EXAFS is a very fast probe (10^{-15} s) and can see similar JT distortions in either the dynamic or static regime. We discuss these and other results mentioned above, in the Discussion section.

So far, there have been few local structure studies done for lower Ca concentration samples, though we have previously shown[13] that the distortion removed as the sample becomes magnetized, is small for a low concentration x ~ 0.12 and very recently Bozin *et al.*[25] have reported on the shortening of the long JT bonds for x from $0-0.5$. However, for samples at the boundary between the ferromagnetic insulator region (Ca concentration below 20%) and the CMR region (Ca concentration $\sim 20-50$ %), no local structure experiments have been done to explore the relationship between distortions removed and the sample magnetization. Here, we present a detailed EXAFS study through the concentration driven metal/insulator transition. We find similar behavior as for LCMO with higher Ca concentrations, but the total distortion removed in the FM insulating state at low T is greatly reduced. Specifically, in a comparison of four different samples (Ca concentrations $0.16-0.22$; effective hole concentrations $y=0.2-0.25$) we find that the total magnitude of the local Mn-O distortions removed in the FM state, decreases rapidly (by more than a factor of 2) when the metal/insulator transition disappears in the resistivity data. For the insulating samples, the small overall change in $\sigma^2(T)$ as the sample becomes magnetized is direct evidence that a large number of Mn sites (at least 50%) have a low distortion per site at T_c.

This paper is organized as follows: a brief description of the data collection and sample preparation are presented in Sec. II, the magnetization and resistivity data are presented in Sec. III, and then the EXAFS data and analysis are discussed in Sec. IV. A comparison with the model of Downward *et al.*[14] and with other results is provided in Sec. V.

II. EXPERIMENTAL DETAILS AND SAMPLE PREPARATION

Transmission EXAFS Mn K-edge data were collected over a wide temperature range ($3-550$ K) on powdered samples at the Stanford Synchrotron Radiation Laboratory (SSRL). A cryostat was used to collect the low temperature ($3-300$ K) data at beamlines 10-2 and 2-3 using both Si(111) and Si(220) monochromators, and an oven was used for the high temperature ($300-550$ K) data at beamline 2-3 using a Si(111) monochromator. To reduce the harmonic content in the x-ray beam, we detuned the monochromator crystals 50%, and also used a harmonic rejection mirror for the Si(220) monochromator on 10-2. The samples are oriented 90° to the x-ray beams. The energy resolution (δE) is 1.0 eV for the Si(111) monochromator and 0.44 eV for the Si(220) monochromator.

Samples of $La_{1-x}Ca_xMnO_3$ with $x=0.16$, 0.18, 0.20, and 0.22 were made by weight appropriate amounts (measured to better than 0.1% of the final metal atom fractions) of 99.99% purity or better La_2O_3, $CaCO_3$, and MnO_2, mixing with a mortar and pestle for 10 min, and reacting for 3 h at 1150 °C in air in an alumina crucible. The samples were removed from the furnace, reground for 10 min, and reacted for 16 h at 1250 °C. This last step was repeated five times with reaction temperatures of 1300 °C, 1350 °C, 1375 °C (twice), and 1400 °C in air. The samples were then reground for 10 min, pressed into pellets, and reacted for 16 h at 1400 °C. The as-made samples $x=0.18-0.22$ showed a metal/insulator transition and had excess oxygen (i.e., a few metal atom vacancies). To lower the O concentration, pressed pellets of the samples were placed in a flow of Ar gas for 12 h at 1250 °C. Iodometric titration was used to determine the final average Mn valence, which was found to be 3.20(1), 3.22(1), 3.23(1), and 3.25(1) for $x=0.16$, 0.18, 0.20, and 0.22, respectively. The excess O is about 0.015 (i.e., $O_{3.015}$), or in terms of metal site vacancies, the composition would be approximately $(La_{1-x}Ca_x)_{0.994}Mn_{0.994}O_3$. Thus the nonstoichiometry is very small. Powder x-ray diffraction revealed the single phase nature of the samples.

Magnetization versus T was measured in a magnetic field of 0.4 T for most samples (0.2 T for the as-made 0.16 and 0.18 samples); M vs B data were also collected at low T. The electrical resistivity was measured on small bars cut from the pressed pellet ($1 \times 1 \times 6$ mm) using a four-probe dc technique.

To prepare EXAFS samples, the pressed pellets were ground in a mortar and pestle, passed through a 400-mesh sieve, and then brushed onto scotch tape for the cryostat measurement, or onto kapton tape for the oven measurement. The tape preferentially holds the smaller grains (≤ 5 μm) in a thin layer; two double layers of tape were used for these EXAFS measurements.

III. MAGNETIZATION AND RESISTIVITY DATA

The magnetization M is plotted as a function of B in Figs. 1(a) and 1(b) for the as-made and Ar annealed samples, respectively. These plots show the evolution of the magnetization process as the hole concentration is lowered. The as-made samples have reached saturation at or below 0.4 T as observed previously for CMR samples.[14,15] However, for the Ar annealed samples the curves are spread out over a range of B fields. Although the $x=0.22$ sample also saturates below 0.4 T, the other samples require significantly larger magnetic fields to reach saturation, and M is still increasing at 1 T for the $x=0.16$ and 0.18 samples. An important question here is whether the lower magnetization at 0.4 T means that some
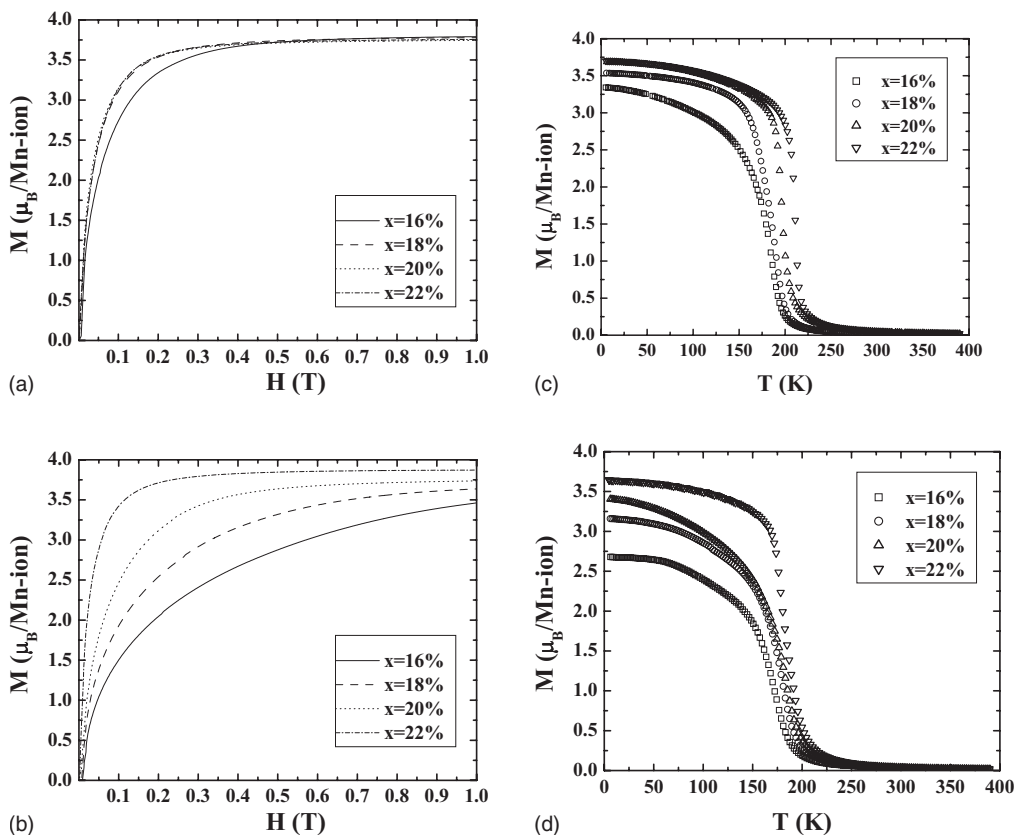
FIG. 1. Magnetization as a function of *B* field and temperature: (a) *M* vs *B* for the as-made samples (5 K), (b) *M* vs *B* for the annealed samples (5 K), (c) *M* vs *T* for the as-made samples (0.4 T for *x*=0.2, 0.22; 0.2 T for *x*=0.16, 0.18), and (d) *M* vs *T* after annealing in Ar (0.4 T). These figures show that the magnetization is highest at low *T* and is fairly close to the theoretically expected value for the as-made samples. For the annealed samples the saturation magnetization is smaller, and significantly reduced for the 16% Ca sample at 0.4 T. Only at high *B* fields does *M* approach the saturated value. The number of data points plotted is reduced to 200 for each curve for clarity.

sites are not yet magnetized or that all the Mn spins are magnetized but some sites are in nonaligned clusters. We argue that it is likely the former. First for all CMR samples the DE-coupled FM sites are easily aligned at 0.4 T and the same should apply for the main FM domains for slightly lower Ca concentrations. However, as the Ca concentration decreases there will be an increasing number of tiny regions with no Ca, and hence no local holes. These nanoscale regions, of order a few unit cells, will possess mostly AFM coupling between a few Mn sites (but no long range AFM order) since that is the dominant magnetic coupling when no holes are present. In addition there will be Mn spins on the boundary between these AFM-coupled nanoclusters and the large FM clusters. Such spins may be frustrated—having AFM coupling to the nano AFM cluster but FM coupling to the FM clusters as a result of occasional hole hopping onto these sites. Consequently, the boundary Mn sites and the AFM-coupled nanoclusters may not be aligned at low *B* fields, but can be forced to align at high *B* fields. The structural results obtained from the EXAFS results below support this scenario and will be discussed in more detail later.

Figures 1(c) and 1(d) show the magnetization *M* as a function of *T* before [Fig. 1(c)] and after [Fig. 1(d)] the anneal in Ar to reduce the O content—the Ca and final hole concentrations are *x*=0.16, 0.18, 0.2, and 0.22, and *y*=0.2,

0.22, 0.23, and 0.25, respectively. Note that the values of T_c are reduced by 15–20 K after the anneal for each concentration. For each plot the saturation magnetization decreases as the Ca concentration decreases whereas a very slight increase is expected [$M_{sat}=(4-x)\mu_B$]; more importantly, the saturation magnetization in the annealed samples is significantly reduced at 0.4 T as discussed above. For the as-made samples the saturation magnetization at low *T* in these plots is low for the *x*=0.16 and 0.18 samples because these data were collected at 0.2 T instead of 0.4 T prior to annealing. For the Ar annealed samples, the saturation magnetization for the 16% Ca sample drops by ∼30% at 4 K (*B*=0.4 T) compared to the 22% sample [Fig. 1(d)].

In Figs. 2(a)–2(d), the resistivity is plotted as a function of *T* for the as-made and Ar annealed samples for each concentration (*x*=0.16–0.22). For the as-made samples, the M/I transition occurs between 0.16 and 0.18 Ca concentration, and $\rho(T)$ varies significantly near T_c. After the reduction of oxygen via the Ar anneal, the resistivity increases considerably and only the 22% Ca sample shows a *M*/*I* transition. From the above data, the annealed samples are mostly in the FM insulator regime and thus are the more important samples for this study. Note that the small reduction in O content has a significant change in the bulk magnetization for the *x*=0.16 sample.
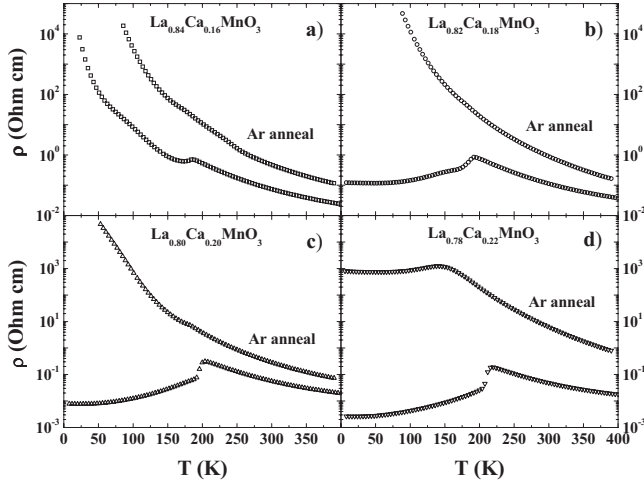
FIG. 2. Plots of the resistivity before and after Ar annealing for the four samples. For the as-made samples, the M/I transition occurs between $x=0.16$ and 0.18; for the Ar annealed samples, only the $x=0.22$ sample shows metalliclike behavior at low T. The number of data points plotted has been reduced to 100 for each curve.

IV. EXAFS DATA AND ANALYSIS

The EXAFS data were reduced using the RSXAP package,[26] which implements standard data reduction techniques. A pre-edge background was removed from the data (the Victoreen formula was used to adjust the slope above the edge after the pre-edge subtraction) and an experimental E_0 was defined as the energy of the half-height point on the Mn K edge. The postedge background was removed using a spline with five knots to approximate μ_0 in $\mu(E) = \mu_0[1 + \chi(E)]$. The background-subtracted data $\chi(E)$ were then transformed to k space using the relation $k = \sqrt{\frac{2m(E-E_0)}{\hbar^2}}$.

Next the k-space data $k\chi(k)$ were fast Fourier transformed (FFT) to r space with a k-space window of $3.3-12.0$ Å^{-1} with a Gaussian broadening of width 0.2 Å^{-1}. Examples of the data are shown in Fig. 3 for two annealed samples ($x = 0.16$ and 0.22).

Fits of the EXAFS data were carried out to the real and imaginary functions in r space [the Fourier transform of $k\chi(k)$], using the EXAFS equation for $k\chi(k)$, which is given by

$$k\chi(k) = \sum_i k\chi_i(k)$$

$$= \operatorname{Im} \sum_i A_i \int_0^\infty F_i(k,r) \frac{g_i(r_{0i},r) e^{i[2kr+2\delta_c(k)+\delta_i(k)]}}{r^2} dr, \quad (1)$$

$$A_i = N_i S_0^2, \quad (2)$$

where $g_i(r_{0i},r)$ is the ith shell pair distribution function (PDF) for atoms at a distance r_{0i} from the center atom (here Mn), $F_i(k,r)$ is the backscattering amplitude, and $\delta_c(k)$ and $\delta_i(k)$ are the phase shifts from the central and backscattering atom potentials, respectively. The amplitude A_i [Eq. (2)], is
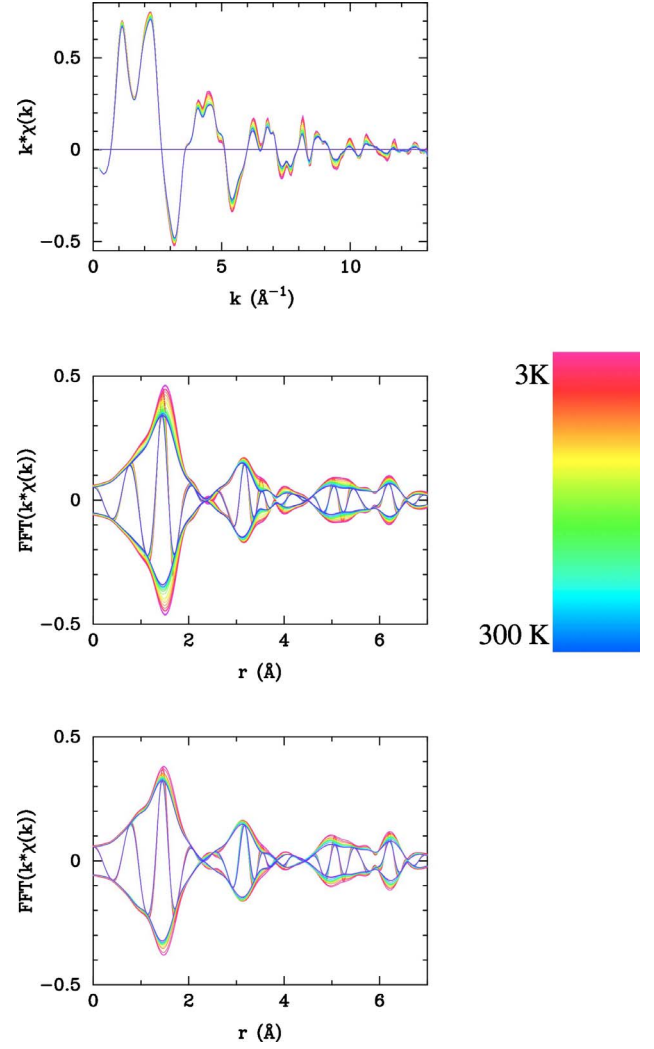

FIG. 3. (Color online) A comparison of EXAFS data for the $x = 0.16$ and 0.22 samples after annealing (hole concentrations are $y = 0.20$ and 0.25, respectively). Top: k-space data for $x = 0.22$. Middle: r-space data for $x = 0.22$. Bottom: r-space data for $x = 0.16$. In each case, the amplitude is highest at low temperature and decreases monotonically with increasing temperature. Note that the amplitude for the $x = 0.16$ sample (bottom) is smaller overall (more disorder) and has a weaker T dependence compared to the $x = 0.22$ sample (middle).

the product of the coordination number N_i from diffraction and S_0^2, the amplitude reduction factor, which is included to correct for multielectron effects since multielectron processes contribute to the edge step height but not to the EXAFS amplitude. Experimentally, S_0^2 also corrects for several other small effects such as small errors in the estimation of the mean-free path in the theoretical calculations, a small amplitude reduction in the data because of the x-ray energy resolution, some harmonic content in the synchrotron beam, nonuniformity or pinholes in powder samples, etc. Finally, an additional parameter ΔE_0 describes the difference in edge energy between the value defined for the data (edge half-height energy) and the theoretical functions described below, for which $k=0$ at E_0.
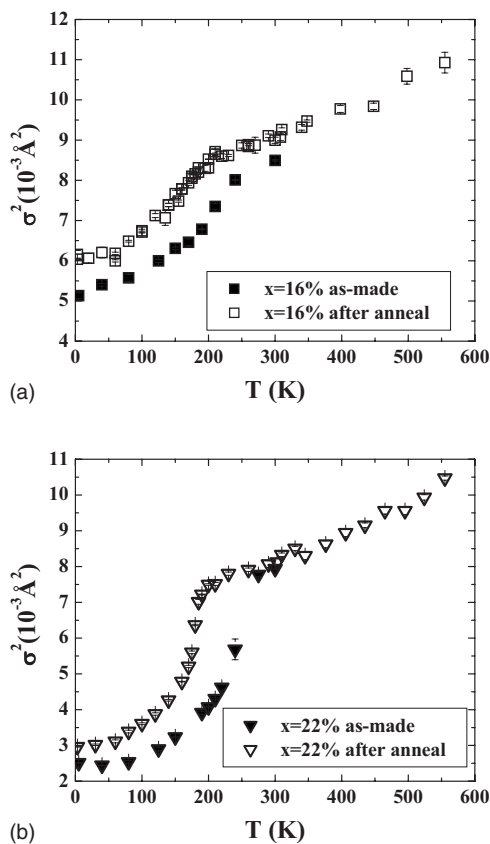
(a)

(b)

FIG. 4. σ^2 as a function of T for (a) $x=0.16$, and (b) $x=0.22$ samples, before and after the Ar anneal. The anneal shifts the step in σ^2 (near T_c) to lower temperatures and the height of the step is reduced. Note the different vertical scales used for (a) and (b).

Since the EXAFS measurements were collected on two different beamlines with different energy resolutions and with two different setups for the low- and high-T ranges, there will be slight variations in the amplitude reduction factor, and we have to choose two slightly different S_0^2 for each set of data as described below, to align the two data sets.

In fitting the EXAFS data, our primary interest is the width of the Mn-O PDF, which parametrizes the amount of distortion present. We used only one value of σ for the Mn-O shell as in previous work,[14] and fixed the number of oxygen neighbors to the lattice structure ($N_1=6$ neighbors) for each sample. Also note that different contributions to σ^2 add up in quadrature if the different distortion mechanisms are uncorrelated; i.e., $\sigma_{total}^2 = \sigma_{phonons}^2 + \sigma_{static}^2 + \sigma_{polarons}^2 + \sigma_{JT}^2$. According to the model proposed by Downward *et al.*,[14] at T_c a fraction $2y$ of the sites are covered by two-site polarons (dimerons) ($\sigma_{polarons}^2$) and the remaining ($1-2y$) are JT distorted electron sites (σ_{JT}^2). These two contributions are summed to give $\sigma_{JT/polarons}^2$; this quantity will vary with magnetization (and temperature) as first the dimerons, and at lower T, the more distorted JT sites, become magnetized.

The data were fit using the program RSFIT (RSXAP package) and theoretical EXAFS functions generated by FEFF 8.20 (developed by Rehr and co-workers[27]). To get a reasonable fit, a number of other constraints on the parameters are also required. First, for data collected on the same sample
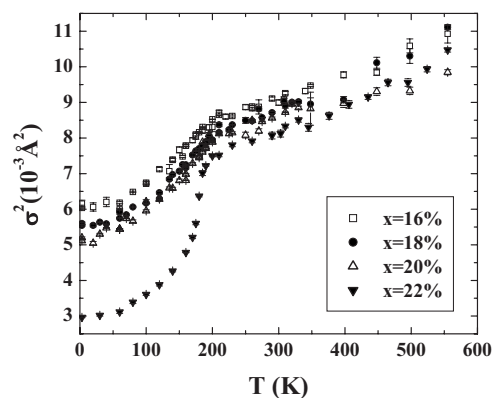

FIG. 5. σ^2 as a function of T for the four annealed samples ($x=0.16-0.22$) on the same vertical scale. The plot of the $x=0.22$ sample is similar to previous samples which show a M/I transition;[14] however, the other three samples, which all show insulating behavior and a reduced saturation magnetization at low T, have a significantly smaller step in σ^2 and a slightly increased distortion above T_c (higher σ^2) than other CMR samples.

and on the same beamline, ΔE_0 was obtained by allowing σ, Δr, and ΔE_0 to vary on the lowest temperature data; the average value obtained from those fits was used to constrain ΔE_0 for the rest of the data in the same set. For the parameter S_0^2, a number of fits were carried out. In the first set of fits, we let the amplitude A_1 ($A_1=N_1 S_0^2$) vary for the low temperature data and determined S_0^2 from those fits. Then A_1 was kept constant for fits as a function of T. The main effect of small changes in this parameter is a vertical shift of plots of σ^2 vs T. Once S_0^2 for the low temperature data (3–300 K) was determined, we slightly adjusted S_0^2 for the high temperature data set (300–550 K) to make the values of σ^2 align with the low T data at 300 K. For all the data below 330 K, $S_0^2 \approx 0.75$; the variation to join high-T and low-T data is ≈ 0.01.

Most of the data were collected on the Ar annealed samples but a few points were collected on two of the as-made samples. In Fig. 4, σ^2 is plotted (on different expanded scales) as a function of T before and after the anneal for $x=0.16$ and 0.22. Although the data for the as-made samples are sparse (solid points), it is clear that after annealing there is a shift of T_c to lower T for both samples (see also Figs. 1 and 2) and that the step height decreases, particularly for the $x=0.22$ sample.

Figure 5 shows $\sigma^2(T)$ for all the annealed samples on the same scale. The step increase in σ^2 is sharp near T_c for the $x=0.22$ ($y=0.25$) sample and has a comparable (slightly smaller) step height to that observed in other CMR samples.[14] As before, we attribute this step to a large increase in the distortions of the Mn-O bonds, associated with dimerons (extended polarons with low distortions) and some more isolated, highly JT-distorted electron sites, as the temperature is increased through T_c. However, the other three samples ($x=0.16-0.20$) have a much smaller step near T_c, which decrease slightly with smaller x, and a much larger value of σ^2 remains at low T. Thus even though a large fraction of the sample is magnetized (70% or more), only a
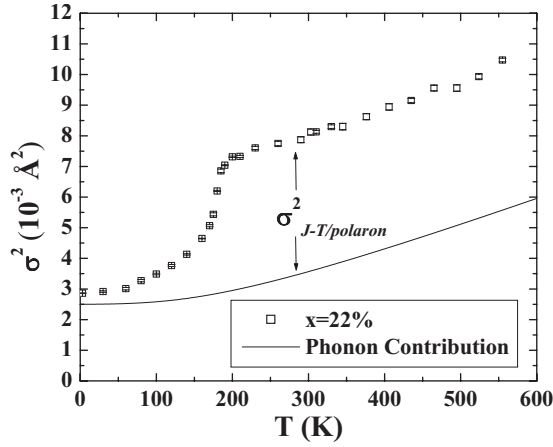
FIG. 6. σ^2 vs T for LCMO, $x=0.22$. The solid line is the phonon contribution calculated using the correlated Debye model with zero static distortion and $\theta_D=830$ K (θ_D for all the samples above T_c varies from 812 to 860 K with an average of about 830 K). $\sigma^2_{JT/polaron}(T)$—the JT/polaron contribution—is defined as the difference between the experimental data and the phonon contribution at each temperature point.

small distortion is removed in the FM phase for these samples. A significant fraction of the sample (up to $\sim 30\%$ for $x=0.16$) remains distorted at the lowest temperatures. [Note: $\sigma^2(4$ K) is well above the value for zero-point motion.] There is also an increased static distortion above T_c for the insulating samples.

In addition, the temperature dependence of $\sigma^2(T)$ above T_c is comparable for all samples. The thermal phonon contributions were determined from a fit of $\sigma^2(T)$ above T_c (205–550 K) to the correlated Debye model [Eq. (3)] plus a static offset. This model is usually a good approximation for all phonon modes[28] including acoustic and optical phonons and is given by[29–31]

$$\sigma^2_{cDebye} = \frac{3\hbar}{2M_R} \int_0^{\omega_D} \frac{\omega}{\omega_D^3} C_{ij} \coth\left(\frac{\hbar\omega}{2k_B T}\right) d\omega, \quad (3)$$

where ω_D is the Debye frequency, C_{ij} is a correlation function given by $1-\sin(\omega r_{ij}/c)/(\omega r_{ij}/c)$, $c=\frac{\omega_D}{k_D}$, where k_D is the Debye wave number, and $\sigma^2_{cDebye}(T\sim 0)$ with zero static offset gives the zero-point motion value of σ^2. The slope of $\sigma^2_{cDebye}(T)$ vs T is very low at low T and increases to a constant value (determined by the spring constant, reduced mass, and C_{ij}) for $T>\Theta_D$. See Ref. 30 for details.

We obtained values of $\Theta_D\sim 812–860$ K± 30 K for the four samples with an average of about 830 K. This agrees well with the value $\Theta_D=860$ K for the Mn-O bond in Ca-substituted LaMnO$_3$ materials as obtained previously.[13,14,32] This fit passes through the points above T_c ($T>200$ K) very well. In Fig. 6, we plot the results for $x=0.22$ and the Debye curve ($\Theta_D=830$ K) with the static contribution removed. This represents the thermal contribution to σ^2 (including zero-point motion); notice that this curve is parallel to the data above T_c.
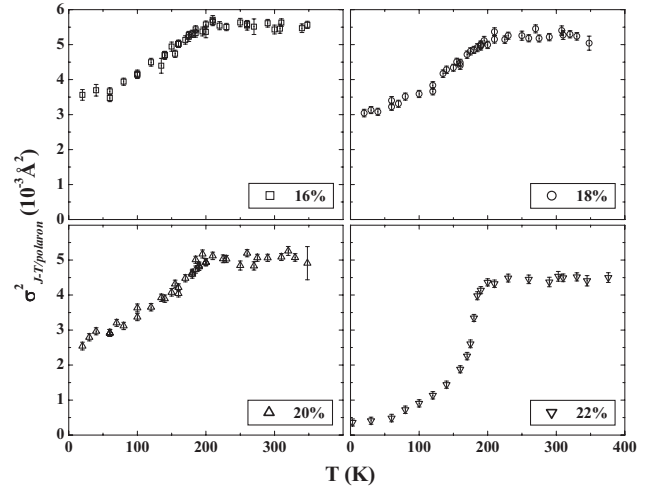

FIG. 7. $\sigma^2_{JT/polaron}(T)$ vs temperature for LCMO $x=16–22$ %. The nonthermal contribution, $\sigma^2_{JT/polaron}(T)$, is defined in Fig. 6. Note that above T_c the $\sigma^2_{JT/polaron}$ is independent of T, and that as the concentration decreases the remaining distortion at low T increases.

The non-thermal-phonon contribution to σ^2 that is removed as the sample is cooled below T_c, $\sigma^2_{JT/polaron}(T)$, can be obtained by subtracting the Debye curve (the solid line in Fig. 6) from the $\sigma^2(T)$ data for each sample. The results are shown in Fig. 7. This plot illustrates several important aspects of $\sigma^2_{JT/polaron}(T)$. First, above T_c it is independent of T—the polaron and JT distortions are fully formed and do not change significantly with T. Second, the step decrease as T goes to zero is greatly diminished for the insulating samples, although the samples are still highly magnetic (see Fig. 1). Third (and related to the second point), the remaining static distortion increases as the Ca concentration is lowered, and as the fraction of the sample that remains unmagnetized at 0.4 T increases.

To investigate the correlations between local structure and magnetization, we plot the data in a way[33] which simplifies the discussion. By combining $\sigma^2_{JT/polaron}(T)$ (Fig. 7) with the $M(T)$ data (Fig. 1) we plot $\sigma^2_{JT/polaron}(T)$ vs $\frac{M}{M_0}$ for the four samples in Fig. 8. Here we use the fraction $\frac{M}{M_0}$ (M_0 is the theoretical saturation magnetization) as an approximate measure of the fraction of magnetized states. At low M, $\sigma^2_{JT/polaron}$ decreases slowly with M, i.e., the distortion removed per Mn site is very small until the sample is at least 50% magnetized. At higher magnetization, $\sigma^2_{JT/polaron}$ drops much more rapidly with M and approaches zero for the 22% sample. However, for the insulating samples, relatively little distortion is removed overall. Note that the slope at low M is similar for all samples, but the 20% and 22% samples have a more continuous change in slope. Here we need to point out one caveat—the EXAFS data were collected at $B=0$ T, while the magnetization data were collected at $B=0.4$ T. We note that while this field is large enough to be reflective of the bulk, zero-field magnetization for CMR samples, it is small enough to have a minimal effect on the magnetoresistance.

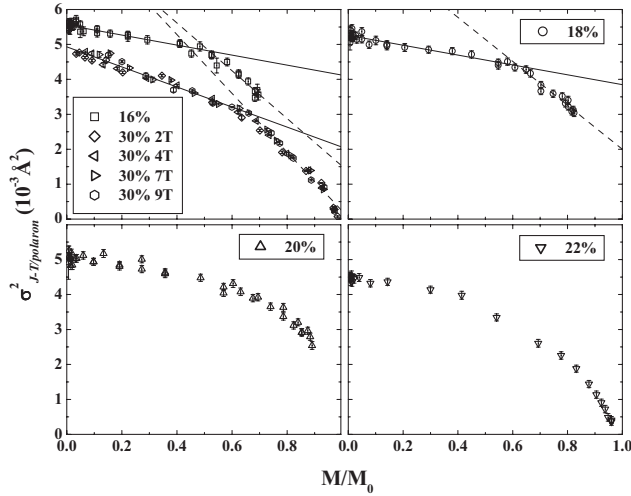Recently, Downward et al.[33] have shown, using EXAFS measurements as a function of magnetic field for four

FIG. 8. $\sigma^2_{JT/polaron}$ vs $\frac{M}{M_0}$ for LCMO $x=16-22$ %. Note that the slope at low M is comparable for all samples and that the JT/polaron distortion is only partially removed for the $x=16-20$ % samples. For comparison, the data for the 30% sample from Downward *et al.*[14] are replotted in this format below the results for the 16% sample.

samples from $21-45$ % Ca, that a universal relationship between the local distortions and the magnetization only exists for high applied B fields, e.g., $B \geq 2$ T. At lower B fields ($B \leq 0.4$ T) for which $|dM/dT|$ is very steep at T_c, domain effects are important and the observed bulk magnetization is lower than expected for the number of magnetized sites implied from the EXAFS data. This analysis suggests that when $|dM/dT|$ is very large at T_c, the $\sigma^2_{JT/polaron}(T)$ vs $\frac{M}{M_0}$ plot becomes more curved and the break-point position varies somewhat with B at low B. For the samples considered here [see Fig 1(d)], the 16% sample has the smallest slope $|dM/dT|$ at T_c, while the 22% sample has the largest; the 18% and 20% slopes are similar. It is only for the 16%, 18%, and possibly the 20% samples that a clear break point near $\frac{M}{M_0} \sim 0.6 \pm 0.1$ is present in Fig. 8, consistent with the previous results for the 21% Ca concentration at higher B field.[14] For the 20% sample, the curve is more rounded but suggestive of a break point between 60% and 70%.

Surprisingly, the magnitude of the slope at low M for the 16% Ca sample (0.0014 Å²) is about a factor of 2 lower than for the 30% Ca sample. For comparison, the 30% data[14] are replotted here, below the data for the 16% sample (Fig. 8);

this suggests that the sites that become magnetized at low M may have even less distortion/site than for the CMR samples. One possibility for this is that the holes are confined to a smaller number of sites and hop rapidly between only a few Mn atoms, keeping them relatively undistorted. A second possible explanation for the low slope at low M is that some of the magnetized Mn sites remain partially distorted and thus less distortion is removed as the sample becomes magnetized. Note that the high M slopes for the low Ca concentration samples ($x=0.16$, 0.18) are comparable (within 25%) to that for the CMR samples. See Table I for a comparison of the high and low slopes with earlier results for CMR samples $x=0.21$ and 0.3.

An important difference for the 16% Ca sample is that the magnetization only reaches $M/M_0 \sim 0.7$ at low T and B =0.4 T. If one extrapolates the straight line through the data from $\frac{M}{M_0}=0.5$ to $\frac{M}{M_0}=1.0$, the distortion that would have been removed if every site became magnetized via DE, is nearly a factor of 2 larger (see the dotted line for the 16% Ca sample in Fig. 8). The remaining JT/polaron distortion at $\frac{M}{M_0}=1.0$, $\sigma^2_{JT/polaron} \sim 1.5 \times 10^{-3}$ Å², is comparable to the excess distortion observed above T_c (Fig. 5) within our uncertainties (in comparison, $\sigma^2_{JT/polaron} \sim 0$ for the 30% sample at $\frac{M}{M_0}$ =1.0). Thus it is as if the magnetization process were truncated for the lower concentration samples before all sites became magnetized.

The small overall distortion removed in the FMI phase for $x=0.16-0.2$, provides direct evidence that low-distortion (nonmagnetized) Mn sites associated with the charge carriers, exist at T_c and are magnetized first. These are possibly the dimeron quasiparticle sites proposed by Downward *et al.*[14] This further supports the proposal that there are at least two types of distorted sites in this system: one associated with the delocalized hole charge carriers (dimeron or two-site polaron) and another with the remaining JT distorted Mn sites.

V. DISCUSSION AND CONCLUSIONS

The first issue to discuss is the structure of these systems above T_c. Neutron diffraction studies show that between 200 and 300 K the samples become pseudocubic and the Mn-O bond lengths are nearly equal above a temperature T_{JT}, at these Ca concentrations.[16,17] In contrast $\sigma^2_{JT/polaron}$ from EXAFS shown in Fig. 7 has a large distortion of the Mn-O PDF above T_c, and it remains constant up to 400 K. Biotteau *et*

TABLE I. Table of slopes from the plots of $\sigma^2_{JT/polaron}$ vs M/M_0. The estimated slope errors are ≤ 20% for the low slope and ≤ 10% for the high slope. The 21% and 30% Ca results are for the high B-field results from Downward *et al.*,[14,33] which have been replotted and analyzed in the same way as in Fig. 8.

Concentration	Low slope (10^{-3} Å²)	High slope (10^{-3} Å²)	Break point	χ^2/ndf [a]
16%	−1.44	−6.84	0.517	0.790
18%	−1.41	−6.29	0.621	1.061
21%	−3.18	−6.31	0.611	4.497
30%	−2.95	−8.65	0.678	2.123

[a]ndf=number of degrees of freedom

al.[16] ascribe this transition to a change from a quasistatic to a dynamic JT effect. We agree with this assignment—EXAFS is a very fast probe ($\sim 10^{-15}$ s) and can follow any structural JT distortions. The constant value of $\sigma^2_{JT/polaron}(T)$ above T_c means that the magnitude of the JT distortion is unchanged. The collapse of the Mn-O PDF observed in neutron diffraction means that the lattice fluctuations associated with JT distortions become faster than the time scale of the neutrons ($\sim 10^{-12}$ s) above T_{JT}. This underscores the importance of including dynamics in any discussion of these systems.

The main results reported above for samples in the FMI regime are (1) the functional relationship between changes in the nonthermal contributions to σ^2 [$\sigma^2_{JT/polaron}(T)$] and the sample magnetization are the same as in the FMM regime; (2) the overall distortion that is removed as the sample becomes ferromagnetic at low T is small (and appears to be significantly smaller for the FMI samples compared to the FMM samples, even for a rather small change in Ca concentration); and (3) a significant fraction of the sample (5–30 % in this concentration range) remains unmagnetized and is still distorted at low T (4 K) at B=0.4 T.

Point (1) suggests that the basic mechanism for FM behavior, which involves the spins, the mobile charges, and the lattice, is the same in both the insulating and metallic FM regimes—thus the DE model (plus local distortions) is also the dominant-coupling mechanism for most of the Mn sites at low Ca concentrations. Point (2) may at first be surprising but the main result is consistent with the earlier results reported by Downward *et al.*[14] for samples in the CMR regime, namely, that there is a large fraction of sites associated with the charge carriers that have a small distortion per Mn site. The small overall distortion/magnetization removed for the x=0.16–0.2 samples is further evidence of this small distortion/site.[14] However, it is not clear from these data why the slopes at low M for the FMI samples in Fig. 8 appear lower than for the CMR sample. The EXAFS studies of the CMR materials by Downward *et al.*[14,33] show that when EXAFS data collected at B=0 are combined with magnetization data at 0.4 T, the slope at low M is smaller than when both EXAFS and magnetization data are collected at high B fields. This will be discussed in more detail in a separate paper.[33]

Point (3) may also be surprising—how does a small fraction of the sample consistently form an insulating layer between more conductive regions? It is perhaps less surprising if one first looks back at the LCMO CMR systems at partial magnetization. From our previous work, the turnover of the resistivity occurs when a significant magnetization has developed; up to that value of magnetization the resistivity is still increasing as T decreases (i.e., an insulator or semiconductor); also, the turnover value of magnetization increases as the Ca concentration decreases. This behavior is comparable to the FM insulator sample with x=0.16, except that turnover does not occur. The difference is that for the CMR sample the most distorted fraction of the sample does become magnetized at lower T—and the sample eventually becomes conducting. For the FMI, much of this fraction remains distorted and never becomes magnetized at 0.4 T. Thus the insulating and metallic systems are quite similar at partial magnetization.

It is useful here to comment further on the issue as to whether at 0.4 T the sample is only partially magnetized or is fully magnetized but many domains are not aligned. Figure 8 shows that at low M the first sites to be magnetized have a low distortion per site. We argue that these sites are related to the DE-coupled FM clusters. If one argues that all sites are magnetized at 0.4 T, then the data for the 16% sample in Fig. 8 should range up to $\frac{M}{M_0}$=1.0 instead of 0.7, the break point would be near 0.75; then there would be an even larger fraction of easily magnetized sites with low distortions which would be inconsistent with the large number of filled e_g sites at low Ca concentrations. The only alternative would be to invoke a FM interaction that would lead to easily magnetized sites at low M that remain highly distorted (and thus have little distortion removed in the magnetized state). This seems unreasonable in view of the properties at slightly higher Ca concentrations.

In their dimeron model, Downward *et al.*[14] suggested that the dimerons are preferentially located along filamentary clusters close to Ca sites; the argument is based on charge neutrality—the dimerons are+charged holes delocalized over two Mn sites while Ca on a La site acts like a negative charge. In such a model the chains of linked unit cells containing a Ca atom form pseudo-one-dimensional filaments within the insulating $LaMnO_3$ host. Once the dimeron sites are magnetized as filamentary clusters, a further increase of magnetization requires magnetizing the surrounding JT distorted Mn sites of the host lattice. Once enough of these sites are magnetized it will connect the filamentary chains and make the sample conducting; however, the smaller the fraction of the sample that forms the filamentary structures, the larger the number of distorted Mn^{+3} (e_g) sites that would need to be magnetized (and be kept undistorted via charge hopping) before the filaments are connected and metallic conductivity can be achieved.

Note that these results again point to an intrinsic inhomogeneity of the material at the level of a few unit cells. One needs to consider nanoscale regions with quite different distortions, that change with the local magnetization—which in turn is determined by changes in T or B. These regions are determined by the distribution of dopants such as Ca, and also on the location of metal atom (Mn, La, etc.) vacancies. It is likely that the poorly defined concentration at which the M/I occurs in LCMO is due to several connected effects— the distribution of Ca, correlations between the location of Ca sites and the location of vacancies, and the dynamics of the charge carriers. The NMR results mentioned in the Introduction[21] suggest that the low-distortion magnetic and high-distortion nonmagnetic regions may be further subdivided into sites with different local B fields but the relative fraction of such sites is not clear.

Although various experiments point towards intrinsic inhomogeneity, it is generally difficult to compare the results for various measurements. However, the EMR microwave spectra (near 9 GHz) do show three different resonances just below T_c—where the EXAFS results also suggest three regions, and we attempt a comparison to these data.[23,24] For the EMR studies it is difficult to determine the volume fraction of the various sites as the double-integrated intensity (DIN)

of the derivative spectra varies dramatically—by a factor of 25—50 near T_c. Further, the microwave fields may not penetrate throughout the sample when significant metallic clusters are present. Therefore, the only EMR quantity for comparison with the EXAFS is the resonance magnetic field.

The strongest resonance line reported[23,24] rapidly moves to zero field for a small decrease in temperature below T_c. Thus for these sites the internal field quickly exceeds the paramagnetic resonance field (about 0.33 T). The EMR authors assume that these sites correspond to the FM metallic regions. In the EXAFS studies,[14] FM metallic regions have essentially zero-polaron distortion; these low-distortion regions also develop rapidly as T is lowered, forming the initially magnetized fraction. Thus the initially magnetized FMM sites (from which a small distortion has been removed in the EXAFS work above) appear to correlate well with the FMM sites identified in the EMR studies.[23,24]

The second line in the EMR studies shifts more slowly towards zero field, and approaches $H=0$ just below 100 K for the 18% and 20% Ca samples. This is the same T range (from T_c to about 75 K) over which most of the polaron distortions are removed (see Fig. 7). Also the T dependence is similar; a fast decrease just below T_c and a slower variation near 100 K. We therefore connect this low field FM EMR signal with the decreasing fraction of unmagnetized polaron sites; the local B field at these sites is increasing with decreasing T, as a result of the growing ferromagnetic magnetization. However, the fraction of such EMR sites cannot be established.

Finally, the EMR studies also show a high field line whose resonance field is well above that for a $g=2$ resonance line. This is suggestive of a local internal field that is opposed to the main ferromagnetic field. It might arise from some Mn sites that are antiferromagnetically coupled within the insulting regions. Thus although the site fraction again cannot be determined, there appears to be a very good correlation between the EMR studies and the EXAFS results.

Resistivity studies also suggest local intrinsic inhomogeneity for the low concentration samples. For the CMR manganites in the FM phase, electrical conduction is often considered to be a percolative problem but it is not simple percolation. If the holes had equal probabilities to be on *any* (Mn) site, then there would be uniform conductivity as is the case for low doping concentrations in n- and p-type semiconductors—and if such a manganite system were 50% magnetized, percolating magnetic clusters would exist across the sample and it would be metallic. Thus there must be preferred hole sites as discussed above. Considering only the Ca dopants, at 20 ± 2 % Ca (the range for the metal/insulator transition) the system is well below the percolation limit for a cubic crystal ($x=0.31$), and even at 25%—well into in the FM-metallic regime—the Ca atoms do not percolate; at these concentrations, chains of Ca atoms form many partially connected filaments but do not have connectivity across the sample. The electrical conductivity, however, depends on the available sites for the hole quasiparticles, which will include Mn sites close to the Ca dopants. This expands the volume of the sample available for conduction to at least one unit cell about each Ca atom but still does not guarantee connectivity as the potentially conductive sites will be fluctuating. How-

ever, if the fraction of conducting sites can be expanded beyond a unit cell (here by making more of the sample ferromagnetic via hole hopping), then these expanded filaments will eventually touch and connectivity can be achieved. For samples close to the metal/insulator transition (either for samples with $x\leq0.2$ at low T or for samples in the CMR regime which are only partially magnetized), the complex conductivity will depend sensitively on the conducting microstructure of the sample.

Finally, we return to the nature of the Mn sites and the hole quasiparticles. In the Introduction we pointed out that if the holes are hopping rapidly on a local scale there will be no Mn^{+4} sites on the time scales of most experiments, but there will be some fully distorted Mn^{+3} sites if these particular Mn sites are rarely visited by a hole—i.e., the holes occupy preferred locations that do not include this subgroup of Mn sites. A large fraction of sites will be an average of occupancy by a hole and by an e_g electron. A hole on a Mn site tends to reduce the local distortion as the JT interaction is not present. When a hole moves off a site (and it now contains an e_g electron) the site will begin to distort since the JT interaction becomes active. Thus such sites will have some average distortion depending on the hopping rate and the time scale of the measurement. EXAFS is a very fast probe (10^{-15} s), much faster than phonon time scales, and will see a weighted average of all the distortions in the sample.

Surprisingly the observed change in the local distortion is small for the first 50% of the sample that becomes magnetized for the CMR samples. This trend continues to be present in samples through the concentration-driven transition from FMM to FMI ($x=0.16-0.22$). A crucial point is that the number of low-distortion sites is far larger than the number of holes and for the low concentration samples, involves a slightly larger number of electron sites. This approximate factor of 2 (number of sites with a low average distortion is $1.5-2.5x$) was the basis for Downward *et al.*[14] to propose the dimeron model. However, note that at any point in time Mn sites occupied by a hole will be in the process of becoming less distorted while the previously occupied site (which now has an e_g electron) will be increasing in distortion. Thus at least two sites are naturally involved. If the hopping is slow enough that the e_g sites become totally distorted before being revisited by a hole then there should be larger distortions removed in the first 50% of magnetization. Alternatively if the hopping is very fast more than two sites may have a low distortion. The small decrease in distortion up to 50% magnetization is thus evidence for fast hopping on a local scale.

Alonso *et al.*[15] also argue for localized Mn^{+4} sites and a reduced JT distortion in the vicinity of Ca dopants, but do not provide a reason for the reduced distortion. The EXAFS confirm that there is a low distortion of many Mn sites— roughly two per Ca site. The number of Mn sites in the vicinity of the Ca atoms is more than $4x$ (note that there are eight Mn neighbor sites per isolated Ca atom, but only four additional Mn neighbor sites for each Ca that is added to an existing linear chain of Ca) and thus the number of low-distortion sites must be more restricted than only counting the number of closest Mn neighbors to Ca. If the hole can hop rapidly back and forth between two (or perhaps three)

sites, it explains the low distortion per site removed for low magnetizations. If the model of Alonso *et al.* is slightly modified to correspond to partially delocalized holes in the vicinity of low JT distortions (i.e., a hole localized over ~ 2 Mn sites) instead of a completely localized Mn^{+4} hole site, then their model becomes identical to the dimeron model.

In summary, the EXAFS data on LCMO samples with Ca concentrations near the metal-insulator transition ($x =0.16-0.22$) show similar behavior at the local scale as do the CMR samples at higher Ca concentrations. The distortions removed in the FM regime are small and show directly that there is a large fraction of low-distortion Mn sites associated with the charge carriers—the proposed two-site polarons (dimeron) sites, or perhaps a more extended polaron distortion. A large fraction of the sample can be magnetized even though the sample is insulating–which is quite similar to the CMR systems at partial magnetization. The unmagnetized fraction is presumably highly distorted.

ACKNOWLEDGMENTS

[1] P. Schiffer, A. P. Ramirez, W. Bao, and S.-W. Cheong, Phys. Rev. Lett. **75**, 3336 (1995).

[2] M. Imada, A. Fujimori, and Y. Tokura, Rev. Mod. Phys. **70**, 1039 (1998).

[3] S.-W. Cheong and H. Y. Hwang, in *Colossal Magnetoresistive Oxides*, edited by Y. Tokura (Gordon and Breach Science Publishers, Amsterdam, 2000), Vol. 2, pp. 237–280.

[4] C. Zener, Phys. Rev. **82**, 403 (1951).

[5] P. W. Anderson and H. Hasegawa, Phys. Rev. **100**, 675 (1955).

[6] P. G. de Gennes, Phys. Rev. **118**, 141 (1960).

[7] A. J. Millis, P. B. Littlewood, and B. I. Shraiman, Phys. Rev. Lett. **74**, 5144 (1995).

[8] A. J. Millis, B. I. Shraiman, and R. Mueller, Phys. Rev. Lett. **77**, 175 (1996).

[9] A. J. Millis, Phys. Rev. B **53**, 8434 (1996).

[10] A. J. Millis, R. Mueller, and B. I. Shraiman, Phys. Rev. B **54**, 5405 (1996).

[11] H. Röder, J. Zang, and A. R. Bishop, Phys. Rev. Lett. **76**, 1356 (1996).

[12] C. H. Booth, F. Bridges, G. H. Kwei, J. M. Lawrence, A. L. Cornelius, and J. J. Neumeier, Phys. Rev. Lett. **80**, 853 (1998).

[13] C. H. Booth, F. Bridges, G. H. Kwei, J. M. Lawrence, A. L. Cornelius, and J. J. Neumeier, Phys. Rev. B **57**, 10440 (1998).

[14] L. Downward, F. Bridges, S. Bushart, J. Neumeier, N. Dilley, and L. Zhou, Phys. Rev. Lett. **95**, 106401 (2005).

[15] J. Alonso, E. Herrero, J. M. Gonzalez-Calbet, M. Vallet-Regi, J. L. Martinez, J. M. Rojo, and A. Hernando, Phys. Rev. B **62**, 11328 (2000).

[16] G. Biotteau, M. Hennion, F. Moussa, J. Rodriguez-Carvajal, L. Pinsard, A. Revcolevschi, Y. M. Mukovskii, and D. Shulyatev, Phys. Rev. B **64**, 104421 (2001).

[17] M. Pissas, I. Margiolaki, G. Papavassiliou, D. Stamopoulos, and D. Argyriou, Phys. Rev. B **72**, 064425 (2005).

[18] P. Dai, J. A. Fernandez-Baca, N. Wakabayashi, E. W. Plummer, Y. Tomioka, and Y. Tokura, Phys. Rev. Lett. **85**, 2553 (2000).

[19] G. Papavassiliou, M. Belesi, M. Fardis, and C. Dimitropoulos, Phys. Rev. Lett. **87**, 177204 (2001).

[20] B. B. Van Aken, O. D. Jurchescu, A. Meetsma, Y. Tomioka, Y. Tokura, and T. T. M. Palstra, Phys. Rev. Lett. **90**, 066403 (2003).

[21] G. Papavassiliou, M. Fardis, M. Belesi, T. G. Maris, G. Kallias, M. Pissas, D. Niarchos, C. Dimitropoulos, and J. Dolinsek, Phys. Rev. Lett. **84**, 761 (2000).

[22] P. A. Algarabel, J. M. DeTeresa, J. Blasco, M. R. Ibarra, C. Kapusta, M. Sikora, D. Zajac, P. C. Riedi, and C. Ritter, Phys. Rev. B **67**, 134402 (2003).

[23] V. Markovich, E. Rozenberg, A. I. Shames, G. Gorodetsky, I. Fita, K. Suzuki, R. Puzniak, D. A. Shulyatev, and Y. M. Mukovskii, Phys. Rev. B **65**, 144402 (2002).

[24] A. I. Shames, E. Rozenberg, G. Gorodetsky, and Y. M. Mukovskii, Phys. Rev. B **68**, 174402 (2003).

[25] E. S. Bozin, M. Schmidt, A. J. DeConinck, G. Paglia, J. F. Mitchell, T. Chatterji, P. G. Radaelli, T. Proffen, and S. J. L. Billinge, Phys. Rev. Lett. **98**, 137203 (2007).

[26] C. H. Booth, *R-Space X-ray Absorption Package*; http://lise.lbl.gov/RSXAP/.

[27] A. L. Ankudinov, B. Ravel, J. J. Rehr, and S. D. Conradson, Phys. Rev. B **58**, 7565 (1998).

[28] N. W. Ashcroft and N. D. Mermim, *Solid State Physics* (Saunders College, Philadelphia, 1976).

[29] P. A. Lee and G. Beni, Phys. Rev. B **15**, 2862 (1977).

[30] B. K. Teo, *EXAFS: Basic Principles and Data Analysis* (Springer-Verlag, New York, 1986).

[31] A. Bianconi, in *X-ray Absorption: Principles, Applications, Techniques of EXAFS, SEXAFS and XANES*, edited by D. C. Koningsberger and R. Prins (John Wiley and Sons, New York, 1988), p. 594.

[32] N. Mannella, A. Rosenhahn, C. H. Booth, S. Marchesini, B. S. Mun, S.-H. Yang, K. Ibrahim, Y. Tomioka, and C. S. Fadley, Phys. Rev. Lett. **92**, 166401 (2004).

[33] L. Downward (unpublished).